Optical Materials 157 (2024) 116310

Contents lists available at ScienceDirect

Optical Materials

journal homepage: www.elsevier.com/locate/optmat

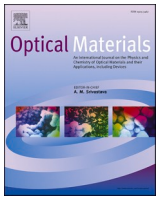

Research Article

Synthesis and thermoluminescence characterization of $Ba_6Y_2W_3O_{18}$ perovskite nanosensors for dosimetry

Soad M. Tadros [a], Mohamed El-Kinawy [b], R. Kamal [a], M. Saif [a], Nabil El-Faramawy [b,*]

[a] Department of Chemistry, Faculty of Education, Ain Shams University, Roxy, 11711, Cairo, Egypt
[b] Department of Physics, Faculty of Science, Ain Shams University, 11566, Abbassia, Cairo, Egypt

ARTICLE INFO

Keywords:
Perovskite
Nanosensor
Thermoluminescence
Dosimetry
Activation energy

ABSTRACT

Through the citrate-assisted sol-gel method, barium gadolinium tungstate ($Ba_6Y_2W_3O_{18}$) perovskite samples were synthesized, and their luminescence properties were investigated. Through X-ray diffraction (XRD) the crystal structure of the prepared samples was examined. The tunnelling electron microscopy (TEM) analysis has confirmed the agglomeration of the nanoparticles into rods with an average diameter and length of 71 and 214 nm, respectively. The thermoluminescence (TL) properties were investigated by; first, estimating the number of composing TL components using both experimental and computational methods; second, studying the dose-response of the glow curves in response to the irradiated beta dose. The third step in the study of the TL properties was to assess the reusability of the prepared samples in TL dosimetry and the fourth step was to estimate the minimum detectable dose of the phosphor samples. The Computerized Glow Curve Deconvolution (CGCD) method was then used to extract the kinetic parameters of the composing TL peaks.

1. Introduction

Thermoluminescence (TL) is a physical phenomenon exhibited by certain natural/artificial crystalline/non-crystalline materials, where they emit luminescence when heated after being previously exposed to ionizing radiation [1–5]. This emitted light is a result of charge carriers (electrons and holes) becoming trapped in defects or impurities during radiation exposure. When the irradiated material is heated, the trapped carriers are thermally released from their energy states, causing them to recombine with holes in color or luminescence centers and emit photons in the form of light. The characteristic proportionality of the emitted light to the amount of radiation absorbed makes TL a valuable technique for quantifying radiation doses and dating objects in fields like archaeology, geology, radiation dosimetry, and forensic science [6–9]. Thermoluminescent dosimeters are commonly used in radiation dosimetry to measure the absorbed dose of ionizing radiation in both humans and materials. It is crucial in various fields, such as medicine, industry, and research, to ensure the safe and effective use of radiation.

Perovskite-based nanomaterials, with their unique structure and properties, have shown great potential in various applications, particularly in chemical and biological sensing [10,11]. Their excellent optical properties, unique sensitivity, selectivity, and long-term stability make them a potential candidate for various applications, such as solar cells, light emitting devices, transistors, sensors, biological detections [11–13].

Tungstate-based double perovskite phosphors are a specific subset of phosphor materials that have the general formula $A_2BB'O_6$, where A is a larger cation (such as a rare earth or an alkaline earth metal), B and B′ are transition metals, and O is oxygen. These materials exhibit unique luminescent properties, used in various applications such as lasers, catalysis, ionic conductors, scintillators, and luminescent materials. Studies have shown that these phosphors exhibit broad excitation spectra in the range of 300–600 nm due to the charge transfer between the elements in the compound, which is important for energy transfer processes relevant to the material's luminescence properties [14,15]. They can have tunable electronic, magnetic, and optical properties, depending on the specific combination of elements and their arrangement in the crystal structure. $Ba_6Y_2W_3O_{18}$ doped with Mg^{2+} and Mn^{4+} exhibits efficient far-red emission around 692 nm, suitable for plant growth due to overlapping with photosensitive pigments [16]. In 2022, Kamal and Saif [17] synthesized and studied the luminescent properties of the new europium-doped barium gadolinium tungstate ($Ba_6Gd_2W_3O_{18}$) perovskite, finding intense luminescence in the red region and highly sensitive and selective to Cu^{2+} ions. It showed a good

* Corresponding author. Physics Department, Faculty of science, Ain shams University, 65511, Abbassia, Cairo, Egypt.
E-mail address: nabil_elfaramawi1@sci.asu.edu.eg (N. El-Faramawy).

https://doi.org/10.1016/j.optmat.2024.116310
Received 29 May 2024; Received in revised form 29 September 2024; Accepted 20 October 2024
Available online 22 October 2024

correlation for copper ion concentration detection over a range of 0.01–100 μm. Wang and Xiao [18] compared the luminescence properties of Mn^{4+} doped $Ba_6Y_2W_3O_{18}$ and $Ba_6Gd_2W_3O_{18}$ phosphors, both with a double perovskite structure. Both phosphors exhibit broad excitation bands and distinct far-red emission bands at 693 nm for the yttrium-based and 676 nm for the gadolinium-based phosphor. The temperature-dependent emission spectra reveals that the BYW:0.006Mn has better thermal stability than that of BGW:0.006Mn. This paper reports for the first time, the synthesis and thermoluminescence characterization of $Ba_6Y_2W_3O_{18}$ perovskite nano sensors for TLD applications.

2. Experimental

2.1. Synthesis

The $Ba_6Y_2W_3O_{18}$ sample was synthesized via a citrate-assisted sol-gel method. Initially, the solution was prepared by mixing 0.006 mol of Ba $(NO_3)_2$ and 0.002 mol of $Y(NO_3)_3$ in 20 mL of distilled water under stirring. Meanwhile, 0.003 mol of $Na_2WO_4.2H_2O$ was dissolved in 10 mL of distilled water in a separate beaker and mixed with the above solution. Then, the above solution stirring for 1 h. After 1-h, citric acid of 0.022 mol (1:2 ratio of metal ions and complexing agent in the composition) was added to the above mixture and the stirring was continued well for 1 h until a homogeneous solution was obtained. The pH value of the solution was adjusted at 7 with the dropwise addition of NH_4OH solution. Then, the solution mixture was heated at 80 °C for 1 h without stirring to form a transparent sol. After that, the sol was left until a wet gel was formed. The wet gel was dried at 120 °C to obtain xerogel. The xerogel was heated at 200 °C for 5 h and then was calcined at 1000 °C for 6 h [17].

2.2. Analytical analyses

The crystal structure was determined by X-ray powder diffraction analysis (XRD), Bruker D8 Advance X-ray diffractometer, Cu Kα radiation (λ = 1.5406 Å) at 10 kV and 10 mA). Additionally, a JEM-2100 (JEOL) model TEM device was used to investigate the nanoparticle size and the elemental contents were examined using EDS detector (Carl Zeiss EVO 18). An American luminescence spectrometer known as the "PerkinElmer LS55″ was used to record the PL studies.

2.3. TL measurements

The TL measurements were conducted using a Lexsyg Smart TL/OSL reader. The reader is equipped with a built-in $^{90}S/^{90}Y$ beta source for irradiation, delivering radiation at a rate of 0.11 Gy/s. The device incorporates a bi-alkaline cathode photomultiplier tube (PMT) (Hamamatsu) for detecting emitted light during TL measurements. Glow curves were recorded using a “wideband” detection window over a temperature range from room temperature (~300 K) to 673 K, using a heating rate of 5 K/s.

2.4. Glow curve analysis

2.4.1. T_m-T_{stop} method

One effective experimental method frequently employed to identify the number of constituent glow peaks is the T_m-T_{stop} method. This method involves irradiating the TL sample with a specified radiation dose, followed by sweeping the glow curve (first TL reading) to a relatively low temperature (T_{stop}), cooling the sample to room temperature (RT), and subsequently performing a second TL reading to record the remaining glow curve. The temperature corresponding to the maximum intensity of the first apparent TL glow peak (T_m) is then determined from the second TL reading.

2.4.2. Computerized glow curve deconvolution

The deconvolution process of the TL glow curves involves separating the composite curve into its individual components or peaks, each corresponding to a specific trapping center within the material. This process is crucial for analyzing and understanding the underlying mechanisms of TL and extracting valuable information on kinetic parameters.

Throughout the current study, a software application employing the Computerized Glow Curve Deconvolution (CGCD) method was utilized to analyze the measured glow curves. This software was developed within the Department of Physics, Faculty of Science, Ain Shams University, Cairo, Egypt [18]. Based on the general-order kinetics model as described in Ref. [10], the CGCD method was employed to deconvolute the TL glow curves. The GO deconvolution equation is given by [10].

$$I(T) = I_M \exp\left(\frac{E}{k\,T}\left(\frac{T-T_M}{T_M}\right)\right) \times \left[1 + \frac{E(b-1)(F(T,E)-F(T_M,E))}{k\,T_M^2\,b\exp\left(\frac{-E}{k\,T_M}\right)}\right]^{\frac{-b}{b-1}} \quad (1)$$

Here, the parameters I_M and T_M refer to the maximum intensity of the glow peak and the corresponding temperature, respectively. The optimization parameter E (eV) represents the thermal activation energy of the corresponding carrier trap, b is the order of kinetics, T (K) is the absolute temperature, and k (J/K) is the Boltzmann constant (8.617E-5 eV/K).

The two functions $F(T,E)$ and $F(T_M,E)$ are given by,

$$F(T,E) = T\exp\left(\frac{-E}{k\,T}\right) + \frac{E}{k}\left(Ei\left(\frac{-E}{k\,T}\right)\right) \quad (2)$$

$$F(T_M,E) = T\exp\left(\frac{-E}{k\,T_M}\right) + \frac{E}{k}\left(Ei\left(\frac{-E}{k\,T_M}\right)\right) \quad (3)$$

Such that, $Ei(-x)$, with x > 0, is the exponential integral function [19].

The frequency factor is calculated using the formula given by,

$$s = \left(\frac{E\,\beta}{k\,T_M^2}\right)\frac{1}{1+(b-1)\left(\frac{2kT_M}{E}\right)}\exp\left(\frac{E}{kT_M}\right) \quad (4)$$

where β is the heating rate.

The physical meaning of the kinetic parameters is illustrated as follows; the peak position, T_M, signifies the location of the trapping center within the bandgap of the material. The frequency factor, s, correlates with the likelihood of thermal excitation of trapped charge carriers from their respective centers. The kinetics order, b, indicates the nature of the trapping center’s emission kinetics, distinguishing between first-order, second-order, or general-order mechanisms.

The figure of merit (FOM) parameter of Balian and Eddy [20], defined by,

$$FOM = \sum_{j_i}^{j_f}\frac{100\left(y_j - y(k_f)\right)}{A} \quad (5)$$

was calculated for each glow curve deconvolution to assess the goodness of the deconvolution process. In equation (6), the parameters j_i and j_f refer to the first and last point in the glow curve, respectively. The parameter y_j represents the experimental TL measured point, $y(k_f)$ is the value of the fitted point, and A is integrated area below the glow curve.

3. Results and discussion

3.1. Crystal structure

The XRD had been usually used for identification of crystal phase and

crystallinity of the prepared materials. The XRD patterns of BYWO synthesized by the citrate-based sol-gel at is shown in Fig. 1. All reflection peaks confirm formation of well-defined crystalline only cubic double perovskite BYWO phase (JCPDS card No. 38–0219) (Wang & Xiao, 2020) and the peaks of 18.30°, 30.14°, 43.30°, 53.61°, 62.60° corresponded to the crystal planes (111), (220), (400), (422), (440) of $BaWO_4$. The crystallite size of the obtained BYWO sample is 82.90 nm by using the Scherrer equation [21]. The lattice parameter of the cubic double perovskite BYWO structure is 8.371 Å that calculated using the plane spacing equation for cubic structure [17,22].

3.2. TEM analysis

TEM image, EDS analysis, high resolution TEM image and SAED pattern of BYWO samples are used for analyzing the morphology and particle size. Fig. 2a–d shows the TEM image, EDS, HRTEM image and SAED patterns of the BYWO sample, respectively. The particles within the BYWO sample exhibit a significant degree of agglomeration nanorods morphology and possess uneven sizes. The average diameter and length are 71 and 214 nm, respectively (Fig. 2a). The EDS analysis (Fig. 2b) of BYWO confirms the existence of barium, yttrium, tungsten, and oxygen elements. The interplanar distances determined from HRTEM image match with the plane (220) for BYWO sample (Fig. 2c). The crystal lattice fringes observed in HRTEM images (0.29 nm) and the bright spots observed in SAED patterns reveal the crystalline nature of the BYWO. Electrons reflected and diffracted from various crystallographic planes of unit cells of BYWO sample produce these bright spots. The diffused rings in the SAED pattern (Fig. 2d) indicate the presence of nanocrystals with different orientation which is in accordance with the XRD results (Fig. 1).

3.3. Spectrum analysis

The emission spectrum of the BYWO under 265 nm excitation wavelength is shown in Fig. 3 it is composed of a broad emission band around 400–600 nm with sharp band at ~480 nm, which is attributed to the intrinsic emission of WO42− groups [17,23].

3.4. T_m-T_{stop} method

To apply the T_m-T_{stop} method in the current study, samples were irradiated with an 11 Gy dose of beta radiation, and the first TL reading was performed from RT to T_{stop} = 328 K. Subsequently, the samples were cooled to RT and subjected to a second TL reading. This cycle was repeated for T_{stop} temperatures ranging from 328 K to 573 K at 5 K intervals. The Tm value obtained at each step was plotted against the corresponding T_{stop} temperature and the resulting plot is shown in Fig. 4. The figure displays the plateau observed in the T_m-T_{stop} experiment, indicating that the recorded glow curve composes of nine TL glow components.

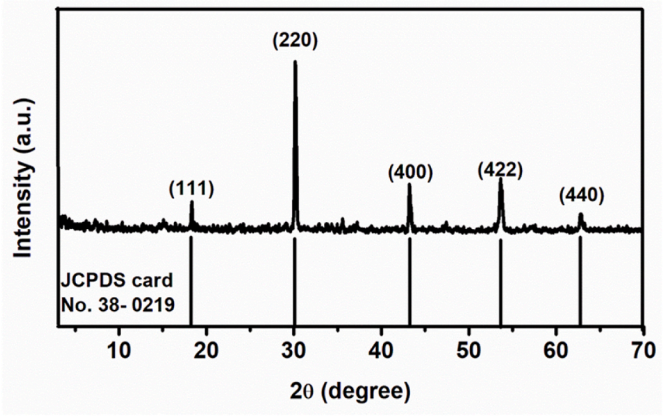

Fig. 1. XRD pattern of the BYWO sample.

3.5. CGCD method

Based on the estimation of the composing peaks, the CGCD method was employed to fit the glow curves to nine TL components and to extract their kinetic parameters. The deconvoluted glow curve of a sample irradiated to a beta radiation dose of 165 Gy is displayed in Fig. 5. The kinetic parameters derived using equations (1)–(4) are presented in Table 1. The activation energies of the charge carrier traps extracted from the TL glow curve ranged from 0.95 to 1.52 eV. The frequency factors associated with the trapping centers were found to lie within the range of E11 and E12. The calculated kinetic orders indicated that most peaks exhibit nearly second-order kinetics, except for peak 1 (P1) showing first-order kinetics and peak 2 (P2) displaying general-order kinetics. The FOM value for the fitting process was 0.34 %, underscoring the reliability of the deconvolution procedure.

3.6. Dose response linearity

Thermoluminescent materials can exhibit various responses to irradiated radiation doses, depending on their composition, structure, and the nature of the radiation. To study the dose-response linearity of the prepared samples, they were irradiated to different beta particle doses in the range from 1.1 Gy to 165 Gy. The integrated areas of the apparent glow curve and the composing TL components versus the irradiated dose are shown in Fig. 6 (note the logarithmic scale on the y-axis). The data of the glow curve/peaks were fitted to an exponential function on the form $y_0 + A\, e^{R_0\, x}$, which corresponds to a linear function in the linear scale, where x is the irradiated dose and R_0 represents the proportionality coefficient between the integrated area and the irradiated dose. The R^2 values of the fitting of the integrated glow curve/peaks were in the range of 0.904–0.999, reflecting the linear response of the integrated area in response to the irradiated beta dose.

3.7. Reusability

To evaluate the suitability of the prepared samples for repeated use as beta dosimeters, a sequence of "irradiation-glow curve readout-background readout" was performed five times, and the resulting glow curve response was analyzed (Fig. 7). The samples were exposed to an 11 Gy dose of β radiation, and the subsequent glow curves were measured and deconvoluted. Fig. 4 presents the integrated areas of the measured glow curves and their components throughout the five cycles. It was observed that the integrated area of the glow curve and TL peaks 1–7 remained relatively stable throughout the cycles. However, the integrated area of peaks 8 and 9 oscillated from one readout to the other, suggesting variability in the response of these specific peaks to repeated measurements.

3.8. Minimum detectable dose

The minimum detectable dose refers to the smallest amount of radiation dose that can be reliably detected and quantified using the TL material [1]. The MDD parameter of the samples under study was estimated using an empirical equation, given by [8].

$$MDD = (B^* + 2\sigma_B)\, F \tag{6}$$

Here, the parameters σ_B, B^*, and F represent the standard deviation of the background of a TL reading obtained from un-irradiated samples, the mean value of these TL readings, and the calibration factor (mGy/nC), respectively. The prepared samples were irradiated to a calibration dose of 11 Gy and the background of the TL signal was recorded five times. The values of the parameters B^* and σ_B were found to be 80267 and

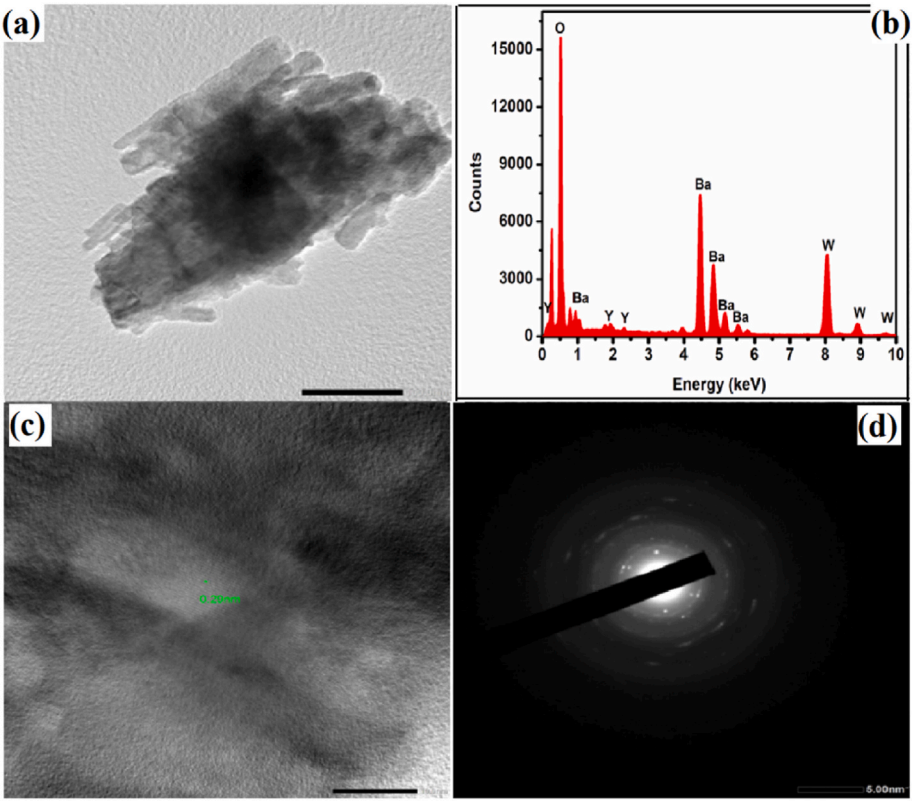

Fig. 2. (a) TEM image, (b) EDS, (c) HRTEM image and (d) SAED patterns of the BYWO sample.

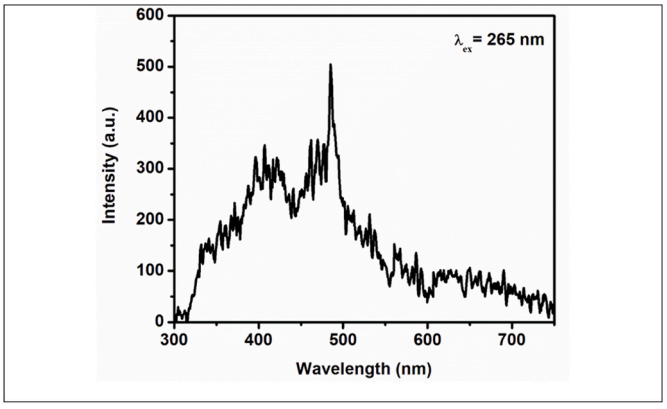

Fig. 3. PL emission spectrum of BYWO sample.

8799.7, respectively. The value of F (= dose (mGy)/A (nC)) was estimated to be 527 E−6. Substituting these values into equation (6) yielded a MDD value of 51.5 mGy.

4. Conclusions

In the current work, barium gadolinium tungstate ($Ba_6Y_2W_3O_{18}$) perovskite samples were synthesized using the citrate-assisted sol-gel method. The XRD analysis confirmed cubic double perovskite BYWO phase of the prepared samples. The morphology of the nano prepared samples was probed using TEM analysis and the formation of rods with an average diameter and length of 71 and 214 nm, respectively, was confirmed.

The experimental and computational glow curve analysis methods estimated the number of TL components that compose the glow curves to be nine. The thermal activation energies of the TL components lie within the energy range of 0.95–1.52 eV. The estimated values of the kinetic orders of the TL components indicated that all the TL peaks follow second-order kinetics, except peaks 1 and 2 showing first- and general-order kinetics behavior, respectively. The displayed glow curves and their composing TL components were found to follow a linear behavior with the irradiated beta radiation in the dose range of 1.1 Gy–165 Gy. The minimum detectable limit of the prepared nano samples was estimated as 51.5 mGy. Accordingly, the prepared nano samples are recommended to be used as beta dosimeters.

A study of the dependence of the TL properties on the preparation

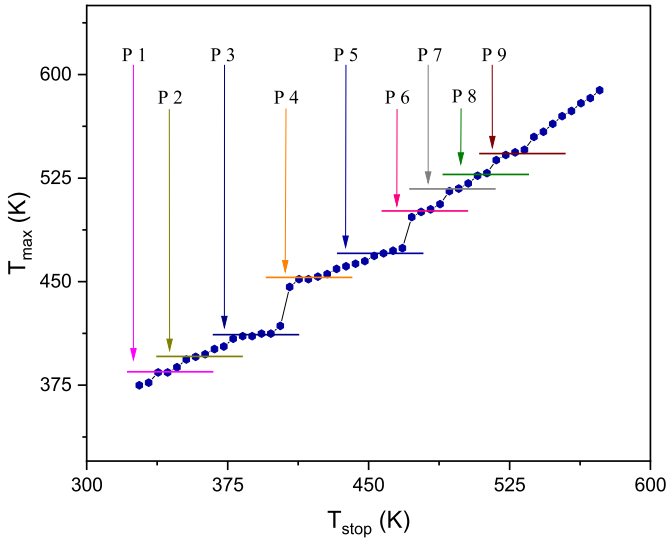

Fig. 4. T_m–T_{stop} plateau of the samples irradiated to an 11 Gy dose of beta radiation.

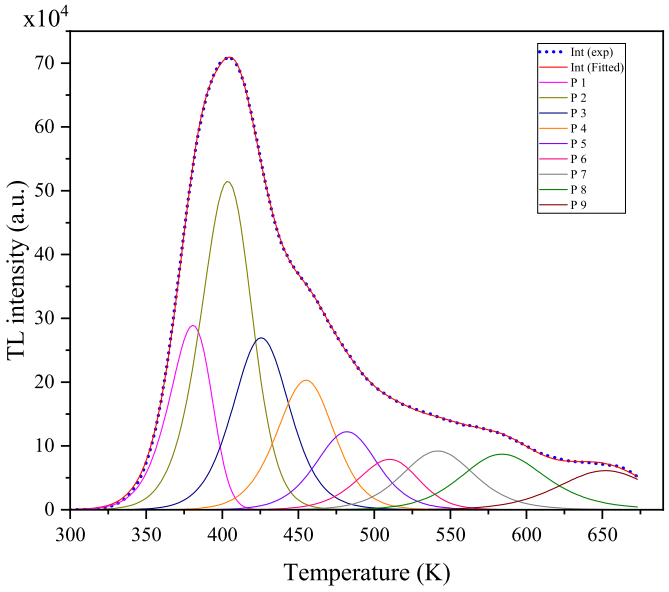

Fig. 5. Deconvolution of the glow curve measured after irradiating the samples to a beta dose of 165 Gy.

Table 1
Kinetic parameters along with the traps' lifetimes obtained using CGCD method of the glass sample.

TL peak #	*E (eV)*	T_M *(K)*	*s* (s^{-1})	*b*	FOM (%)
1	0.95	380.7	1.42E+12	1.16	0.34
2	1.01	403.6	1.38E+12	1.47	
3	1.10	425.6	3.74E+12	1.74	
4	1.21	455.1	8.76E+12	1.64	
5	1.29	482.0	9.69E+12	1.70	
6	1.35	510.1	6.49E+12	1.48	
7	1.43	541.8	5.28E+12	1.83	
8	1.49	583.9	1.59E+12	1.98	
9	1.52	652.0	1.16E+11	1.66	

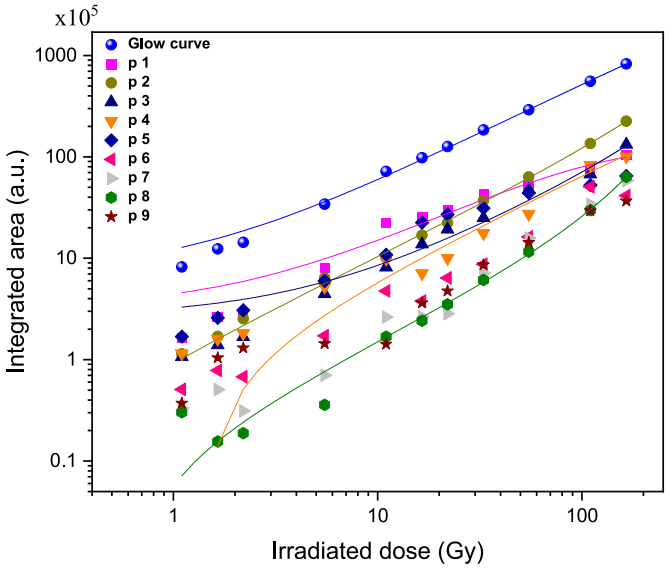

Fig. 6. Integrated area below each TL glow peak after irradiating the prepared samples with beta radiation doses in the range of 1.1–165 Gy.

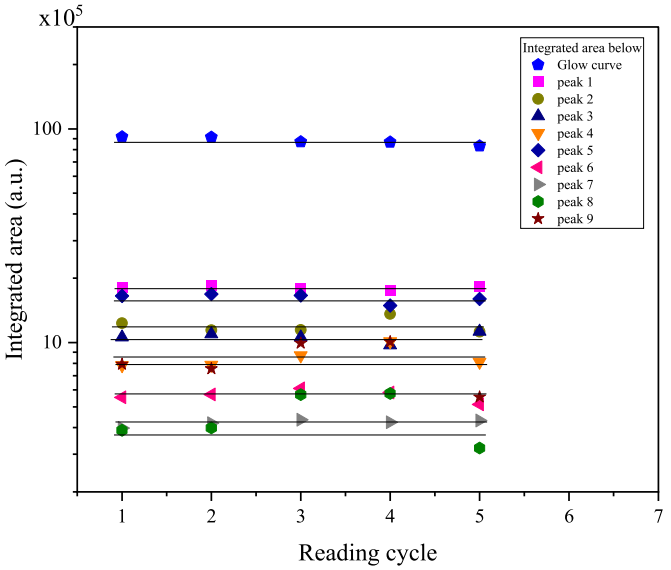

Fig. 7. Reusability (TL glow curve/peak area vs. reading cycle) of the prepared samples irradiated with an 11 Gy dose of beta particles.

conditions, like calcination temperature and/or synthesis method, requires much extensive work which is beyond the objective of the current study. For example, previous studies prepared UO_2^{2+} doped SrHfO3 perovskite samples using solid-state diffusion method [24], Eu^{3+} doped Sr_2YVO_6 double perovskite using high-temperature combustion synthesis [25], Ca_3WO_6 doped with Er^{3+}, and Mn^{4+} doped $Ba_6Y_2W_3O_{18}$ & $Ba_6Gd_2W_3O_{18}$ using solid-state reaction methods [26,27] and they have shown that the different prepared perovskite samples displayed photo and thermoluminescence response to beta irradiation.

Though there is unprecedented improvement of solvent engineering technology for synthesizing this perovskite crystal of good quality. However, the single-step solution process suffers from the inherent difficulties of producing Perovskite thin film of various morphology due to the uncontrolled synthesis process. Thus, one should opt for better ways of producing perovskite crystal of uniform morphology.

CRediT authorship contribution statement

Soad M. Tadros: Writing – original draft, Investigation. **Mohamed El-Kinawy:** Writing – original draft, Software, Methodology, Investigation, Data curation. **R. Kamal:** Methodology. **M. Saif:** Writing – review & editing. **Nabil El-Faramawy:** Writing – review & editing, Data curation, Conceptualization.

Declaration of competing interest

The authors declare that they have no known competing financial interests or personal relationships that could have appeared to influence the work reported in this paper.

Data availability

Data will be made available on request.

References

[1] S.W.S. McKeever, Thermoluminescence of Solids, Cambridge University Press, London, 1985.
[2] N. El-Faramawy, A. El-Naggar, C. Woda, M. El-Kinawy, Investigation of TL dosimetric parameters of lithium borate glass doped with dysprosium, Opt, Materials 113 (2021) 110672.
[3] N. El-Faramawy, H. Alazab, S. Rawash, N. Diab, M. El-Kinawy, Passive dosimetry of β-irradiated lithium borate doped glass, Opt. Mater. 120 (2021) 111472.

[4] M. El-Kinawy, F. Abdel-Wahab, N. El-Faramawy, Luminescence characterizations of highly beta sensitive lithium silicate systems, Opt. Mater. 145 (2023) 114378.
[5] N. El-Faramawy, M. Sabry, S. Farouk, M. El-Kinawy, A. Mafodda, C. Woda, Preliminary study of lithium tetraborate doped with Cu and in for external dosimetry, Appl. Radiat. Isot. 191 (2023) 110533.
[6] S. Farouk, H. Al-Azab, A. Gad, H. El-Nashar, N. El-Faramawy, Thermoluminescence response and its kinetic analysis of a natural milky quartz associated with tin-tungsten-fluorite mineralization, Radiat. Phys. Chem. 181 (2021) 109333.
[7] W.L. McLaughlin, Trends in Radiation Dosimetry, Pergamon Press, Oxford, 1982.
[8] C. Furetta, Handbook of Thermoluminescence, World Scientific Publishing Co. Pte. Ltd, Singapore, 2010.
[9] K.V.R. Murthy, Thermoluminescence and its applications: a review, Defect Diffusion Forum 347 (2013) 35–73.
[10] M. Enhessari, A. Salehabadi, M. Enhessari, A. Salehabadi, Perovskites-based nanomaterials for chemical sensors, Chapter (4) in "Progresses in Chemical Sensor" Oen Access Book, 2016.
[11] M. Shellaiah, K.W. Sun, Review on sensing applications of perovskite nanomaterials, Chemosensors 8 (3) (2020) 55.
[12] S. Ahmad, A. Husain, M.M. Ali, K.I. Khana, A. Khancd, A.M. Asiricd, Perovskite-based Material for Sensor Applications, Hybrid Perovskite Composite Materials: Design to Applications, 2021, pp. 135–145.
[13] V. Vasylkovskyi, I. Bespalova, M. Slipchenko, O. Slipchenko, Y. Zholudov, B. Chichkov, Review: electrochemiluminescence of perovskite-related nanostructures, Crystals 13 (2023) 455.
[14] P. Niu, X. Liu, Z. Xie, W. Zhao, Photoluminescence properties of a novel red-emitting nanowire phosphor $Ba_6Gd_2W_3O_{18}$:Eu3+, J. Lumin. 198 (2018) 34–39.
[15] W. Wang, S. Xiao, Comparative investigation on luminescence properties of Mn^{4+} doped $Ba6Y_2W_3O_{18}$ and $Ba_6Gd_2W_3O_{18}$ phosphors, Mater. Res. Bull. 123 (2020) 110709.
[16] F. Zhou, F. Qiu, C. Wang, S. Xin, M. Gao, Z. Li, G. Zhu, Synthesis and photoluminescence properties of double perovskite phosphor $Ba6Y_2W_3O_{18}$: Mg^{2+}, Mn^{4+} for plant cultivation, ECS J. Solid State Science and Tech. 8 (10) (2019) 119–126.
[17] R. Kamal, M. Saif, Down shifting luminescent Eu^{3+} doped $Ba_6Gd_2W_3O_{18}$ perovskite Nanosensor for Cu^{2+} ions in drinking water and food samples, J. Photochem. Photobiol., A 429 (2022) 113939.
[18] M. El-Kinawy, H. El-Nashar, N. El-Faramawy, New designed software to deconvolute the thermoluminescence glow-curves, SN Appl. Sci. 1 (2019) 834.
[19] Erdelyi, Tables of Integral Transforms, vol. II, McGraw Hill, New York, 1954.
[20] H.G. Balian, N.W. Eddy, figure-of-merit (fom), an improved criterion over the normaized chi-squared test for assessing goodness-of-fit of gamma-ray spectral peaks, Nucl. Instrum. Methods 145 (1977) 389.
[21] U. Holzwarth, N. Gibson, The Scherrer equation versus the 'Debye-Scherrer equation', Nat. Nanotechnol. 6 (2011) 534–1534.
[22] Z. Ghubish, R. Kamal, Hala R. Mahmoud, M. Saif, H. Hafez, M. El-Kemary, Novel fluorescent nano-sensor based on amino-functionalization of Eu^{3+}:$SrSnO_3$ for copper ion detection in food and real drink water samples, RSC Adv. 11 (2021) 18552–18564.
[23] M.H. Li, L.L. Wang, W.G. Ran, Z.H. Deng, C.Y. Ren, J.S. Shi, Tunable emission of single-phased $NaY(WO_4)_2$:Sm^{3+} phosphor based on energy transfer, Ceram. Int. 43 (2017) 6751–6757.
[24] S.K. Gupta, M. Tyagi, K. Sudarshan, Stabilization of UO^{22+} in $SrHfO_3$ perovskite and probing defects, local structure and photo/thermoluminescence, J. Lumin. 243 (2022) 118663.
[25] N. Degda, N. Patel, V. Verma, K.V.R. Murthy, N. Chauhan, M. Singhal, M. Srinivas, Photoluminescence and thermoluminescence kinetic features of Eu^{3+} doped Sr_2YVO_6 double perovskite phosphor, Opt. Mater. 142 (2023) 114019.
[26] N. Degda, N. Patel, K. Chaudhari, K.V.R. Murthy, N. Acharya, M. Srinivas, Photoluminescence and beta-ray irradiation induced thermoluminescence of Er(III) doped tungstate double perovskite, Phys. B Condens. Matter 691 (2024) 416301.
[27] W. Wang, S. Xiao, Comparative investigation on luminescence properties of Mn^{4+} doped $Ba_6Y_2W_3O_{18}$ and $Ba_6Gd_2W_3O_{18}$ phosphors, Mater. Res. Bull. 123 (2020) 110709.